Canadian Journal of Chemistry

Article

NMR characterization of novel interactions between p97 AAA+ ATPase and the p47 adaptor revealing insights into substrate delivery mechanism

Peter Kim[a], **Megan Black**[a], **Felipe Perez**[b], **and Rui Huang**[a,c]

[a]Department of Chemistry, University of Guelph, Guelph, ON N1G 2W1, Canada; [b]Signal 1 AI, Toronto, ON M5R 2E3, Canada; [c]Department of Molecular and Cellular Biology, University of Guelph, Guelph, ON N1G 2W1, Canada

Corresponding author: **Rui Huang** (email: rhuang08@uoguelph.ca)

Abstract

p97/VCP is an essential AAA+ ATPase involved in diverse cellular activities by interacting with an array of protein adaptors that recruit p97 for specific tasks. p47 is one of the adaptors that targets p97 for membrane remodeling by forming a stable complex with p97 through multivalent interactions. Here, we report a pair of previously unidentified interactions between the N-terminal part of p47 (residues 1–94) and the N-terminal domain (NTD) of p97. Using nuclear magnetic resonance (NMR) spectroscopy, we identify two binding sites on p47, one located on the ubiquitin-associated (UBA) domain and the other on the intrinsically disordered linker, that interact with the same basic patch on p97 NTD, driven by electrostatic forces. Reciprocal NMR titration experiments between p47 (residues 1–94) and p97 NTD reveal that these interactions are relatively weak in nature with dissociation constants on the order of hundreds of micromolar to millimolar *in trans*. Structural models of the two interactions are developed based on NMR chemical shift perturbations, which reveal details of the tentative binding interfaces. Our findings provide new insights into the mechanism by which ubiquitinated substrates are delivered from p47 to p97 for unfolding.

Key words: p97/VCP, p47, p97 adaptor, protein–protein interaction, NMR, intrinsically disordered, biomolecular complex

1. Introduction

p97, also known as the valosin-containing protein (VCP), is a highly conserved and abundant AAA+ (ATPase Associated with diverse cellular Activities) enzyme that participates in a variety of cellular functions spanning from protein quality control to cell cycle regulation and membrane remodeling.[1–4] p97 utilizes the chemical energy released from ATP hydrolysis to power substrate extraction and unfolding in various contexts. It plays a pivotal role in maintaining protein homeostasis and thus has emerged as a highly promising target in cancer therapy, as many cancer cells are reliant on p97 and other proteostasis factors to survive.[5–7] Missense mutations of the p97 gene have been implicated in several neurodegenerative disorders, including multisystem proteinopathy type 1,[8] familial amyotrophic lateral sclerosis,[9] vacuolar tauopathy,[10] and Charcot–Marie–Tooth disease (CMT2Y),[11] underscoring its significant role in cellular physiology.

p97 functions as a homo-hexamer, with each protomer encompassing two tandem ATPase domains (D1 and D2) organized into coaxially stacked rings enclosing a central channel, along with an amino (N)-terminal domain (NTD) localized to the periphery of the D1 ring (Fig. 1A). p97 displays six-fold rotational symmetry in the substrate-free form with the NTDs adopting either an "up" conformation when bound with an ATP analogue or a "down" conformation in the presence of ADP.[12,13] Recent strides in structural studies of the substrate-bound conformation of p97 and its homolog, Cdc48, have unveiled that the protomers of p97 form a right-handed spiral when the substrate is engaged.[14–17] These structures reveal a processive, "hand-over-hand" mechanism for substrate translocation, by which sequential ATP hydrolysis and binding propels the movement of the p97 protomer from the bottom of the spiral to the top, thus driving substrate advancement through the channel. Notably, this mechanism appears to be conserved among a number of AAA+ translocases.[18]

Crucial to p97's functional versatility is its interaction with over 30 adaptor proteins, channeling it to diverse subcellular locations and substrate targets.[3,19–21] Among these adaptors, p47, the first identified p97 adaptor, directs p97 towards membrane remodeling tasks such as post-mitotic reassembly of the Golgi apparatus.[22–24] p47 is a monomeric protein comprised of three folded domains connected by long flexible linkers (Fig. 1B).[25–27] The ubiquitin regulatory X (UBX) domain, structurally similar to ubiquitin, is known to bind to the NTD of p97,[28] while the ubiquitin-associated (UBA) domain recruits ubiquitinated substrates to the complex.[29,30] The biological function of the Shp, eyc, and p47 (SEP) domain in p47 is still elusive, yet it is proposed to be involved

Fig. 1. Domain organization of p97, p47, and the p47 variants. (A) Domain architecture of a p97 promoter (top) and sphere representation of the hexameric p97 in the ADP-bound state (bottom) (PDB ID code 5FTK).[12] (B) Domain architecture of the full-length mouse p47. Structures of the folded domains—the ubiquitin-associated (UBA) (orange) (PDB ID code 1V92),[25] Shp, eyc, and p47 (SEP) (purple) (PDB ID code 1VAZ),[25] and ubiquitin regulatory X (UBX) (green) (PDB ID code 1S3S)[28] domains, are shown in cartoon depictions below, while the positions of the linear motifs, including the SEP-interacting motif (SIM) (blue), SHP_N (yellow), and SHP_C (red), are indicated by boxes. The truncated N-terminal fragment $p47_{1–94}$, used in this study, is presented in (C). NTD, N-terminal domain.

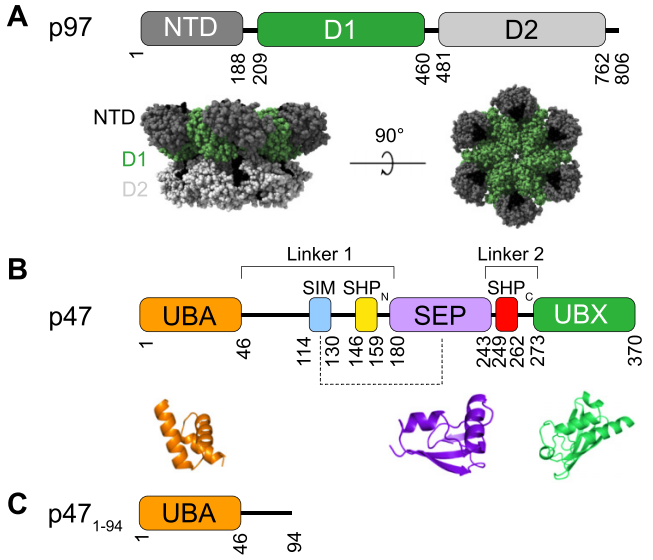

in the direct binding of a substrate in a homologous p37–p97 complex.[31] Notably, on the flexible linkers of p47 reside two linear motifs, namely SHP_N and SHP_C, that also play critical roles in the p47–p97 interaction (Fig. 1B). A previous nuclear magnetic resonance (NMR) spectroscopy study revealed that the SHP_C motif binds to the same NTD of p97 as the UBX domain, while the SHP_N motif interacts with an adjacent NTD depending on the nucleotide-state of p97.[32] Furthermore, a recent cryoEM structure of the p97–p47 complex provided important mechanistic insights into the substrate translocation process.[14]

While these advances have greatly enhanced our comprehension of the p97–p47 interaction, the precise means by which the complex delivers ubiquitinated substrates into p97's central pore for unfolding remains enigmatic. The UBA domain of p47 has been shown to directly bind mono-ubiquitin and plays a central role in substrate tethering.[29] A structural model of the p47 UBA-ubiquitin complex has been proposed based on NMR chemical shift measurements.[28] However, there exists a lengthy linker spanning 134 amino acids between the UBA domain and the SEP-UBX domains which are anchored on the top of the p97 ring (Fig. 1B, Linker 1). This sequential arrangement presents a potential challenge in efficiently delivering the substrate to p97's central pore for processing. Owing to the inherent flexibility of Linker 1 and the UBA domain, the cryoEM map of the p97–p47 complex did not yield observable density for the UBA domain,[14,32] making it difficult to elucidate the mechanism underlying the transfer of substrates from p47 UBA to p97. Intriguingly, a linear motif named SIM (SEP-Interacting Motif) (Fig. 1B), located in Linker 1, has been discovered to interact with the SEP domain,[32] potentially limiting the conformational space that the linker can sample and aiding in substrate delivery. Furthermore, an additional linear region in Linker 1 spanning residue 69–92 was found to inhibit the ATPase activity of p97, while removal of this stretch turns p47 from an inhibitor to an activator of p97.[33] Building upon these observations, we hypothesize that additional interactions exist between the N-terminal fragment of p47, namely the UBA domain and the following linker region, and p97, potentially steering UBA's conformational dynamics for effective substrate delivery. In this study, we present structural characterization of the interaction between the N-terminal fragment of p47 (residue 1–94), referred to as $p47_{1–94}$ hereafter, and the NTD of p97 ($p97_{NTD}$) using solution NMR spectroscopy. NMR chemical shift perturbation (CSP) analysis reveals two novel binding sites on $p47_{1–94}$ that interact with $p97_{NTD}$, one of which resides on an acidic patch of the UBA domain while the other site spans residues 76–90 on Linker 1. Detailed analysis of the interface residues on $p47_{1–94}$ and $p97_{NTD}$ suggests that the binding is mainly driven by electrostatic interaction. Using a shorter construct $p47_{1–61}$ (residue 1–61), we confirm that the two binding sites on $p47_{1–94}$ interact with an overlapping region on $p97_{NTD}$. Reciprocal NMR titrations between $p47_{1–94}$ and $p97_{NTD}$ are carried out to characterize the binding affinities, and dissociation constants of 1.73 ± 0.22 and 0.794 ± 0.057 mM are obtained for the two independent binding events, respectively, from global fitting of the two sets of titration data. Finally, restraints from NMR CSPs are used to calculate structural models of the complexes formed by the two interactions using HADDOCK. Our results highlight the multivalent nature of the interaction between p97 and the p47 adaptor. Importantly, these newly discovered interactions may provide important insights into how the ubiquitinated substrates are delivered from the UBA domain of p47 to the p97 central pore for unfolding and translocation.

2. Materials and methods

2.1. Cloning and protein expression

The expression plasmids of $p97_{NTD}$ (residues 1–213) and $p47_{1–94}$ (residues 1–94) were generated from the full-length *Mus musculus* p97 in a pET28b vector[34] and the full-length *Mus musculus* p47 in a pET29 vector,[32] respectively, with Phusion DNA polymerase (New England Biolabs) using the QuikChange site-directed mutagenesis method (Agilent, Santa Clara, CA, USA). Both constructs contain an N-terminal His_6-tag and a tobacco etch virus (TEV) cleavage site between the tag and the protein. All proteins were expressed in *Escherichia coli* BL21(DE3) cells (New England Biolabs).

To produce unlabeled proteins, transformed cells were grown in LB media containing 50 μg/mL kanamycin at 37 °C until protein expression was induced with 0.25 mM IPTG at $OD_{600} = 0.7$ and continued for ~18 h at 25 °C. Before isotope labeling of the proteins, small-scale expression trials were first carried out in unlabeled M9 minimal media to determine the optimal IPTG concentration, expression temperature, and post-induction duration to obtain the highest expression level in M9 minimal media. Expression of the target proteins was assessed using SDS-PAGE and compared between various conditions. For uniformly ^{15}N-labeled $p47_{1–94}$ and $p97_{NTD}$, proteins were expressed in M9 minimal media with $^{15}NH_4Cl$ as the sole nitrogen source. Transformed cells were first inoculated in a few milliliters of LB broth and grown until $OD_{600} = \sim 0.7$ before being transferred to a small volume (1/10 of the final volume of the culture) of M9 minimal media at a starting OD_{600} of 0.1. Note that cells were pelleted and resuspended with M9 media before being transferred, while the residual LB broth was discarded. The small M9 culture was grown for 16 h at 37 °C before being directly transferred into the full culture and grown at 37 °C until protein expression was induced at $OD_{600} = 0.7$. To express ^{15}N-labeled $p47_{1–94}$, cells were induced with 1 mmol/L IPTG and grown at 37 °C for 6 h before harvest, while for ^{15}N-labeled $p97_{NTD}$ 0.25 mM IPTG was used to induce protein expression followed by growth at 37 °C for approximately 18 h.

2.2. Protein purification

Cells were harvested via centrifugation at 4347 × *g* for 45 min subsequently resuspended in Ni-A buffer (50 mM Tris-HCl (pH 7.4), 30 mM imidazole, and 500 mM NaCl). Approximately 1 mg of lysozyme was added to the resuspended cells, followed by lysis through sonication. After centrifugation at 11 139 × *g* for 30 min, the supernatant was applied to 5 mL of HisPur™ Ni-NTA Resin (ThermoScientific). The column was then washed with Ni-A buffer to remove proteins nonspecifically bound to the column, and the target protein was eluted with Ni-B buffer (25 mM Tris-HCl (pH 7.8) and 300 mM imidazole). Subsequently, TEV protease was added to the Ni eluate to cleave the His_6-TEV-tag (~1:50 molar ratio of TEV protease to the target protein), followed by dialysis against a buffer containing 50 mM Tris-HCl (pH 7.5), 100 mM NaCl, 1 mM EDTA, and 2 mM DTT overnight at 4 °C. The cleaved His_6-tag, TEV protease which contains an uncleavable His_6-tag, and the uncleaved target protein, were then removed by applying the protein solution to a second Ni affinity column and collecting the flow-through. Further purification of the proteins was accomplished using a Superdex 75 Increase 10/300 column (GE Healthcare) in a buffer containing 50 mM HEPES (pH 7.5), 100 mM NaCl, and 1 mM EDTA. After purification, protein samples were exchanged into the NMR buffer (25 mM Bis-Tris (pH 6.6), 25 mM NaCl, 1 mM EDTA, and 10% D_2O) using an Amicon centrifugal concentrator (Millipore) before NMR measurement or were frozen with liquid nitrogen and stored at −80 °C for storage. The purities of the samples were assessed to be >95% based on analyses of the SDS-PAGE results (Fig. S1A) using Image Lab (Bio-Rad). The concentrations of the proteins were measured using absorbance at 280 nm with extinction coefficients predicted from the primary sequences of the constructs using Expasy ProtParam tool. The mass of ^{15}N-labeled $p47_{1–94}$ was confirmed using mass spectrometry (Fig. S1B).

2.3. NMR experiments

All NMR experiments were performed on a 600 MHz Bruker Avance III NMR spectrometer equipped with a 5 mm TCI cryoprobe. All the ^{15}N-^{1}H HSQC spectra were acquired at 25 °C with an interscan delay of 1.5 s, acquisition times of 39 and 64 ms, and 70 and 640 complex points, in the t_1 and t_2 dimensions, respectively. Carriers were positioned in the centre of the water resonance (~4.673 ppm) and 119 ppm for ^{1}H and ^{15}N, respectively. All NMR spectra were processed using NMRPipe[35] and visualized using NMRFAM-SPARKY.[36]

To obtain binding affinities of the interactions between $p47_{1–94}$ and $p97_{NTD}$, two sets of NMR titration experiments were carried out in which (*i*) unlabeled $p97_{NTD}$ was added to a solution of ^{15}N-labeled $p47_{1–94}$ (maintained at 54 μM) in a series of six steps at a total concentration of 0, 0.334, 0.784, 1.20, 1.60, and 2.00 mM $p97_{NTD}$, respectively, and (*ii*) unlabeled $p47_{1–94}$ was added to a solution of ^{15}N-labeled $p97_{NTD}$ (maintained at 100 μM) in a series of 12 steps at a total concentration of 0, 0.153, 0.306, 0.463, 0.618, 0.773, 0.927, 1.08, 1.24, 1.39, 1.55, and 1.70 mM $p47_{1–94}$, respectively. To obtain the CSP of $p97_{NTD}$ upon binding to $p47_{1–61}$, ^{15}N-^{1}H HSQC spectra of 65 μM ^{15}N-labeled $p97_{NTD}$ were recorded in the presence and absence of 1.45 mM $p47_{1–61}$.

2.4. Analysis of NMR data

2.4.1. Chemical shift perturbation

Average CSPs were calculated from the ^{15}N-^{1}H HSQC spectra according to

$$\text{CSP}_{av} = \left\{\Delta\delta_H{}^2 + (0.14 \times \Delta\delta_N)^2\right\}^{0.5} \quad (1)$$

in which $\Delta\delta_H$ and $\Delta\delta_N$ are chemical shift differences (ppm) in the ^{1}H and ^{15}N dimensions, respectively.[37]

2.4.2. Fitting K_d using a one-site binding model

Assuming a one-site binding model $A + B \rightleftharpoons AB$, K_d was extracted from nonlinear least squares fits of the individual titration profile of each residue using the following equation:

$$\text{CSP}_{av} = \text{CSP}_{max}\frac{P_T + L_T + K_d - \sqrt{(P_T + L_T + K_d)^2 - 4P_TL_T}}{2P_T} \quad (2)$$

where CSP_{av} is the CSP for a specific peak calculated using eq. 1, CSP_{max} is the chemical shift difference between the free and fully bound states of the ^{15}N-labeled titrate, and P_T and L_T are the total concentrations of the ^{15}N-labeled titrate and the unlabeled titrant, respectively. Fitting was performed using an in-house Python script. Uncertainty of the K_d values was obtained from the covariance matrix.

2.4.3. Global fitting of the reciprocal titrations between $p47_{1–94}$ and $p97_{NTD}$

Assuming the interactions of $p47_{Site\ I}$–$p97_{NTD}$ and $p47_{Site\ II}$–$p97_{NTD}$ are independent, a two-site binding model is described by

$$(3)\quad p47_{Site\ I} + p97_{NTD} \rightleftharpoons p47_{Site\ I} \cdot p97_{NTD} \quad K_1$$

$$(4)\quad p47_{Site\ II} + p97_{NTD} \rightleftharpoons p47_{Site\ II} \cdot p97_{NTD} \quad K_2$$

where K_1 and K_2 are the association constants for the two binding events, respectively. Based on eqs. 3 and 4, the concentrations of the bound populations, therefore, can be written as

$$(5)\quad [p47_{Site\ I} \cdot p97_{NTD}] = K_1\,[p47_{Site\ I}]\,[p97_{NTD}]$$

$$(6)\quad [p47_{Site\ II} \cdot p97_{NTD}] = K_2\,[p47_{Site\ II}]\,[p97_{NTD}]$$

Since each $p47_{1–94}$ molecule contains two binding sites—Site I and Site II, the total concentration of Site I (or Site II) is equivalent to the total concentration of $p47_{1–94}$, which is the sum of the free and bound forms, described by

$$(7)\quad [p47_{1–94}]_T = [p47_{Site\ I}]_T = [p47_{Site\ I} \cdot p97_{NTD}] + [p47_{Site\ I}]$$

$$(8)\quad [p47_{1–94}]_T = [p47_{Site\ II}]_T = [p47_{Site\ II} \cdot p97_{NTD}] + [p47_{Site\ II}]$$

where $[p47_{1–94}]_T$ is the total concentration of $p47_{1–94}$, $[p47_{Site\ I}]_T$ (or $[p47_{Site\ II}]_T$) is the total concentration of Site I (or Site II), $[p47_{Site\ I}]$ (or $[p47_{Site\ II}]$) is the concentration of the free Site I (or Site II), and $[p47_{Site\ I} \cdot p97_{NTD}]$ (or $[p47_{Site\ II} \cdot p97_{NTD}]$) is the concentration of Site I (or Site II) that is bound to $p97_{NTD}$.

At the same time, the total concentration of $p97_{NTD}$ is written as

$$(9)\quad [p97_{NTD}]_T = [p47_{Site\ I} \cdot p97_{NTD}] + [p47_{Site\ II} \cdot p97_{NTD}] + [p97_{NTD}]$$

CSPs of $p47_{Site\ I}$ (CSP_1), $p47_{Site\ II}$ (CSP_2), and $p97_{NTD}$ (CSP_3) are written as

$$(10)\quad CSP_1 = CSP_{1,max}\,[p47_{Site\ I} \cdot p97_{NTD}]\,/[p47_{1–94}]_T$$

$$(11)\quad CSP_2 = CSP_{2,max}\,[p47_{Site\ II} \cdot p97_{NTD}]\,/[p47_{1–94}]_T$$

$$(12)\quad CSP_3 = CSP_{3,max}[p47_{Site\ I} \cdot p97_{NTD}]/[p97_{NTD}]_T + CSP'_{3,max}[p47_{Site\ II} \cdot p97_{NTD}]/[p97_{NTD}]_T$$

in which $CSP_{1,max}$ and $CSP_{2,max}$ are the chemical shift differences between the free and fully-bound states of the $p47_{Site\ I}$ and $p47_{Site\ II}$, respectively, and $CSP_{3,max}$ and $CSP'_{3,max}$ are the chemical shift differences between the free $p97_{NTD}$ and its fully-bound states saturated with $p47_{Site\ I}$ and $p47_{Site\ II}$, respectively.

Equations 5–12 were fitted globally to obtain K_1 and K_2 using an in-house Python script employing the PyTorch package for minimization.[38] Distributions and uncertainties of the fitted K_1 and K_2 values were obtained from running 100 Bootstrap simulations.[39]

2.5. Structural modeling for the $p47_{1–94}$–$p97_{NTD}$ complex

Structural models of the $p47_{1–94}$–$p97_{NTD}$ complex were calculated using HADDOCK2.4 webserver with NMR CSPs input as ambiguous restraints for docking.[40,41] To obtain a structural model of the Site I-$p97_{NTD}$ complex, the NTD in the crystal structure of mouse p97 (PDB ID 1R7R)[42] and the AlphaFold-predicted structure of the UBA domain (residues 1–49) in mouse p47[43] were used as input structural files. 19 residues in $p97_{NTD}$ (L17, K18, Q19, N24, R25, K60, G61, K62, K63, R64, R65, E80, V166, I189, K190, R191, E192, E196, and L198) and 7 residues in Site I of p47 (A39, Y42, E43, D44, G45, E48, and D49) were input as active residues. To model the Site II-$p97_{NTD}$ complex, $p97_{NTD}$ (PDB ID 1R7R)[42] and the AlphaFold-predicted structure of $p47_{1–94}$[43] were used as input structural files. The same 19 residues in $p97_{NTD}$ as listed above and 7 residues in Site II of p47 (R76, D77, I79, Q82, E85, E86, and E90) were input as active residues. For the Site II-$p97_{NTD}$ complex, residues 75–90 of $p47_{1–94}$ were set to be fully flexible throughout the entire docking protocol except for the rigid body minimization step so as to account for intrinsic dynamics as well as the relatively low confidence in the predicted structure of this region by AlphaFold. The active residues were selected as they showed significant CSPs (1 STD above average) upon interaction with the binding partner. Passive residues that correspond to surface neighbors of the active residues in $p97_{NTD}$ and $p47_{1–94}$ were selected automatically by the HADDOCK webserver using the default criteria of >15% solvent accessibility and >1 atom within 6.5 Å from an active residue. Docking was run under default parameters unless otherwise specified.

3. Results and discussion

3.1. The N-terminal region of p47 interacts with $p97_{NTD}$ via two novel binding sites

Previous studies have revealed that several regions in the full-length p47 interact with p97, namely the SHP_N motif (residues 146–159), the SHP_C motif (residues 249–262), and the UBX domain (residues 273–370).[14,27,28,32] To explore potential weak binding that originates from the N-terminal region of p47 and eliminate interferences from previously identified strong interaction sites, we chose to use a construct of p47 containing only residues 1–94 ($p47_{1–94}$) (Fig. 1C) in this study and characterize its potential interaction with the NTD of p97. The NTD of p97 was selected because a vast majority of p97 adaptors interact directly with the NTD, while the conformational switch of the p97 NTD that accompanies ATP hydrolysis appears to regulate the interactions between p97 and some of its adaptors.[34,44–46]

We first expressed ^{15}N-labeled $p47_{1–94}$ and recorded the ^{15}N-^{1}H HSQC spectra. A comparison between the ^{15}N-^{1}H HSQC spectrum of $p47_{1–94}$ and that of the full-length p47 recorded in a previous study[32] (Fig. S2A) shows very small chemical shift differences for residues 1–94 between the two spectra (Fig. S2B). This highlights the modular nature of p47 and allows us to confidently transfer the backbone assignments of residues 1–94 from the full-length p47 to the trun-

cated construct $p47_{1–94}$ (Fig. S3). Figure 2A shows the ^{15}N-^{1}H HSQC spectra of $p47_{1–94}$ in the presence and absence of a 30-fold excess of $p97_{NTD}$. We observed CSPs for a subset of backbone amides, while the majority of the resonances in the spectra remained unchanged, indicating specific interaction between $p47_{1–94}$ and $p97_{NTD}$. Plotting CSP against the protein sequence shows that residues with significant CSPs (1 standard deviation above the average) are clustered in two regions of $p47_{1–94}$—residues A39, Y42, E43, D44, G45, E48, and D49, which are located at the C-terminal half of α3 in the UBA domain and the following linker region (Fig. 2B, Site I, cyan), and residues R76, D77, I79, Q82, E85, D86, and E90, which are located at the C-terminal of the linker in this construct (Fig. 2B, Site II, cyan). Mapping these residues onto the structure of $p47_{1–94}$ (Fig. 2C, middle) revealed that the interaction sites are focused on two conserved acidic patches of the construct (Fig. 2C, bottom; Fig. 2D), suggesting the interaction may be driven by electrostatic energy. Interestingly, Site II has been previously reported to be an inhibitory motif for p97 ATPase and Golgi reassembly activity.[33]

To assess the affinity of the interaction, we performed an NMR titration experiment, in which increasing concentrations of unlabeled $p97_{NTD}$ were added to ^{15}N-labeled $p47_{1–94}$ and the CSPs were monitored as a function of $p97_{NTD}$ concentration (Fig. 2E). We first used a naïve one-to-one binding model to fit the individual titration profiles and extracted the apparent dissociate constant, $K_{d,\,app}$, for each residue, as described in the "Materials and methods" section. Table S1 lists the fitted $K_{d,\,app}$ values for residues with significant CSPs in $p47_{1–94}$. An average $K_{d,\,app}$ of 1.41 ± 0.18 and 0.701 ± 0.127 mM were obtained for residues located in Site I and Site II, respectively. The significant difference in the apparent affinities between residues at the two binding sites suggests two distinct binding events, with Site II binding $p97_{NTD}$ with a relatively higher affinity than Site I.

3.2. The two binding sites on $p47_{1–94}$ interact with overlapping regions on $p97_{NTD}$

To determine the binding interface on $p97_{NTD}$, we expressed ^{15}N-labeled $p97_{NTD}$ and transferred the assignment of the backbone amide resonances from a previous study (Fig. S4).[32] We recorded ^{15}N-^{1}H HSQC spectra of $p97_{NTD}$ in the presence and absence of a 17-fold excess of unlabeled $p47_{1–94}$ and observed CSPs for a subset of specific residues (Fig. 3A). Significant CSPs were observed for residues I16, L17, K18, Q19, N24, R25, K60, G61, K62, K63, R64, R65, E80, V166, I189, K190, R191, E192, E196, and L198 (Fig. 3B), which are clustered mainly in three regions of $p97_{NTD}$, including the unstructured N- and C- terminal regions as well as a basic loop in the N-lobe of the NTD (Fig. 3C, top). These residues form a localized and continuous surface on $p97_{NTD}$ (Fig. 3C, middle, yellow), while mapping electrostatic potential on the surface reveals that the residues involved in the interaction with $p47_{1–94}$ all reside in a distinct basic patch in $p97_{NTD}$ (Fig. 3C, bottom). Notably, significant CSPs were observed in acidic regions of $p47_{1–94}$ upon interaction with $p97_{NTD}$ (Fig. 2C). These observations again imply that the interaction between $p97_{NTD}$ and $p47_{1–94}$ is driven by electrostatic energy, and both acidic sites on $p47_{1–94}$ bind to the same basic patch on $p97_{NTD}$. To quantify the binding affinity, we carried out a second set of NMR titration experiment in which unlabeled $p47_{1–94}$ was titrated to ^{15}N-labeled $p97_{NTD}$ and the CSPs were monitored as a function of $p47_{1–94}$ concentration (Fig. 3D). Fitting the individual titration profiles with a simple one-to-one binding model yielded $K_{d,\,app}$ values (Table S2) that follow a normal distribution with an average of 0.229 ± 0.068 mM (Fig. S5), which also suggests an overlapping binding interface on $p97_{NTD}$ for both binding sites on $p47_{1–94}$.

To distinguish the two binding events, namely between Site I or II on $p47_{1–94}$ and $p97_{NTD}$, we employed a further truncated construct of p47 (residue 1–61, Fig. 4A) with Site II removed. Figure 4B shows the CSP of residues in $p97_{NTD}$ upon the addition of a 22-fold excess of unlabeled $p47_{1–61}$. Residues that show significant CSPs upon binding to $p47_{1–61}$ (Fig. 4B) are largely overlapped with those upon binding to $p47_{1–94}$ (Fig. 3B) and located in the same basic patch on the surface of $p97_{NTD}$ (Fig. 4C, orange). This confirms that the two binding sites on $p47_{1–94}$ (Site I and II) interact at an overlapping region on $p97_{NTD}$. Therefore, Site I and Site II are likely to compete for the same binding surface on $p97_{NTD}$, and for a given $p97_{NTD}$, the binding of either Site I or Site II is mutually exclusive.

3.3. Global fitting of the NMR titrations

To obtain a quantitative description of the two interactions, we globally fitted the two sets of NMR titration data between $p47_{1–94}$ and $p97_{NTD}$ using a two-site binding model, as described in the "Materials and methods" section, assuming that the two binding events are independent. Global fitting results in dissociate constants of 1.73 ± 0.22 and 0.794 ± 0.057 mM for the Site I – $p97_{NTD}$ and Site II-$p97_{NTD}$ interactions, respectively, suggesting the interactions are weak *in trans*. It is worth noting that, in the context of full-length p47 and p97, other interactions between p47 and p97, i.e., binding of the UBX domain and SHP motifs to p97 with submicromolar K_ds, effectively tether p47 onto p97. As a result, the interactions between $p97_{NTD}$ and Site I or II should be more prominent *in cis* due to increased local concentrations of the binding partners and reduced entropic penalty relative to the case of bimolecular association.

3.4. Structural modeling reveals novel interactions between p47 and $p97_{NTD}$

Based on NMR CSP analysis, we used a HADDOCK approach to calculate the structural model of the $p47_{1–94}$ – $p97_{NTD}$ complex.[40,41] Due to the lack of structure for the full-length p47, we used the AlphaFold predicted structure of $p47_{1–94}$ (Fig. S6) as a structural input for docking. The complex models for $p47_{Site\ I}$ – $p97_{NTD}$ and $p47_{Site\ II}$ – $p97_{NTD}$ were calculated separately, as detailed in the "Materials and methods" section. We selected the clusters of the final structures for the two complexes based on the lowest HADDOCK scores and the largest cluster sizes. For the $p47_{Site\ I}$ – $p97_{NTD}$ complex, the lowest energy structure from the selected cluster (Fig. 5A) shows that the binding interface on p47 mainly consists of α3 (including L34, Q35, L38, A39, S40, Y42, E43, D44, D47,

Fig. 2. The N-terminal part of p47 weakly interacts with $p97_{NTD}$. (A) Superposition of ^{15}N-^{1}H HSQC spectra of ^{15}N-labeled $p47_{1-94}$ in the presence (orange) and absence (dark green) of a 30-fold molar excess of unlabeled $p97_{NTD}$ (left), illustrating site-specific chemical shift perturbation (CSP) of $p47_{1-94}$ upon addition of $p97_{NTD}$. Selected regions in the boxes (left, dashed lines) are enlarged on the right. (B) CSP from ^{15}N-^{1}H HSQC spectra of $p47_{1–94}$ resulting from the addition of $p97_{NTD}$. The average CSP value and CSP 1 STD above the average are indicated with solid and dashed lines, respectively. (C, top) Domain architecture of $p47_{1–94}$ with the two regions that show significant CSPs upon binding to $p97_{NTD}$ denoted in cyan boxes. (C, middle) Surface representation of $p47_{1–94}$ (AlphaFold prediction)[43] with residues that show significant CSPs colored in cyan. (C, bottom) Surface representation of $p47_{1–94}$ colored by electrostatic potential using UCSF ChimeraX.[48] (D) Sequence alignment for Site I and II in p47. Numbering is consistent with full-length mouse p47. (E) Averaged CSPs of the $p47_{1–94}$ amide groups titrated with $p97_{NTD}$. Titration curves are shown for residues A39, D44, and G45, which are located in UBA, and residues E85, E86, and E90, which are located in the linker. Each curve was individually fit to a simple one-site binding model. NTD, N-terminal domain; UBA, ubiquitin-associated.

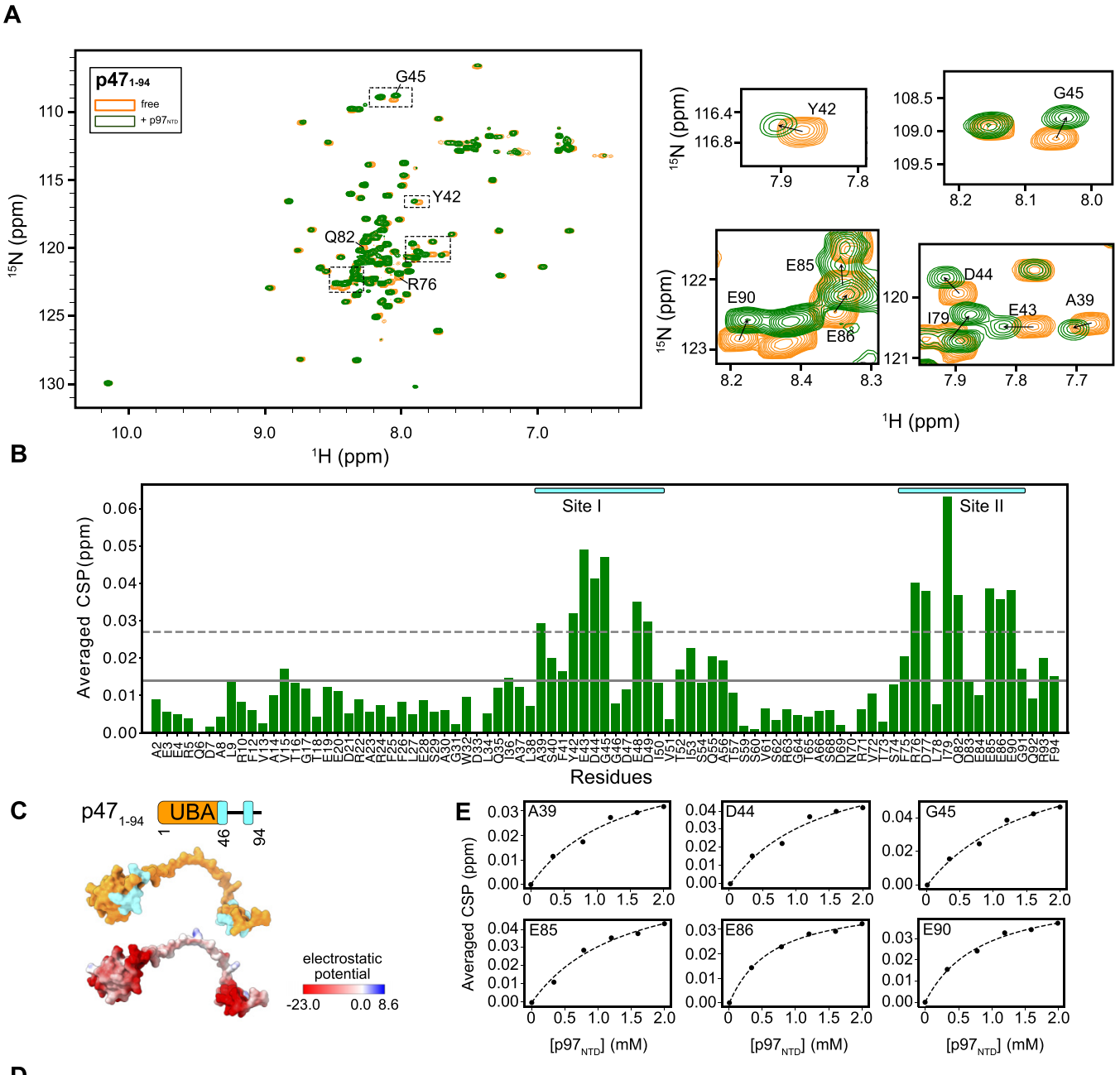

Fig. 3. Mapping the interaction site on $p97_{NTD}$ upon binding to $p47_{1–94}$. (A) Superposition of ^{15}N-^{1}H HSQC spectra of ^{15}N-labeled $p97_{NTD}$ in the presence (light green) and absence (pink) of a 17-fold molar excess of unlabeled $p47_{1–94}$ (left). Selected regions in the boxes (left, dashed lines) are enlarged (right). (B) Chemical shift perturbations (CSPs) from ^{15}N-^{1}H HSQC spectra of $p97_{NTD}$ upon addition of $p47_{1–94}$. The average CSP value and CSP 1 STD above average are indicated with solid and dashed lines, respectively. Residues with CSPs 1 STD above the average are annotated. (C) Cartoon (top) and surface (middle) representations of $p97_{NTD}$ (PDB ID code 1R7R,[49] residue 1–213) with residues that show significant CSPs (1 STD above average) in (B) colored in yellow. (Bottom) A Coulombic surface presentation of $p97_{NTD}$, colored based on electrostatic potential using UCSF ChimeraX,[48] shows that the binding site on $p97_{NTD}$ is mainly located on a basic patch. (D) Averaged CSPs of the $p97_{NTD}$ amide groups titrated with $p47_{1–94}$. Titration curves are shown for residues I16, L17, N24, K63, R64, and E192. Each curve was individually fit to a simple one-site binding model. NTD, N-terminal domain.

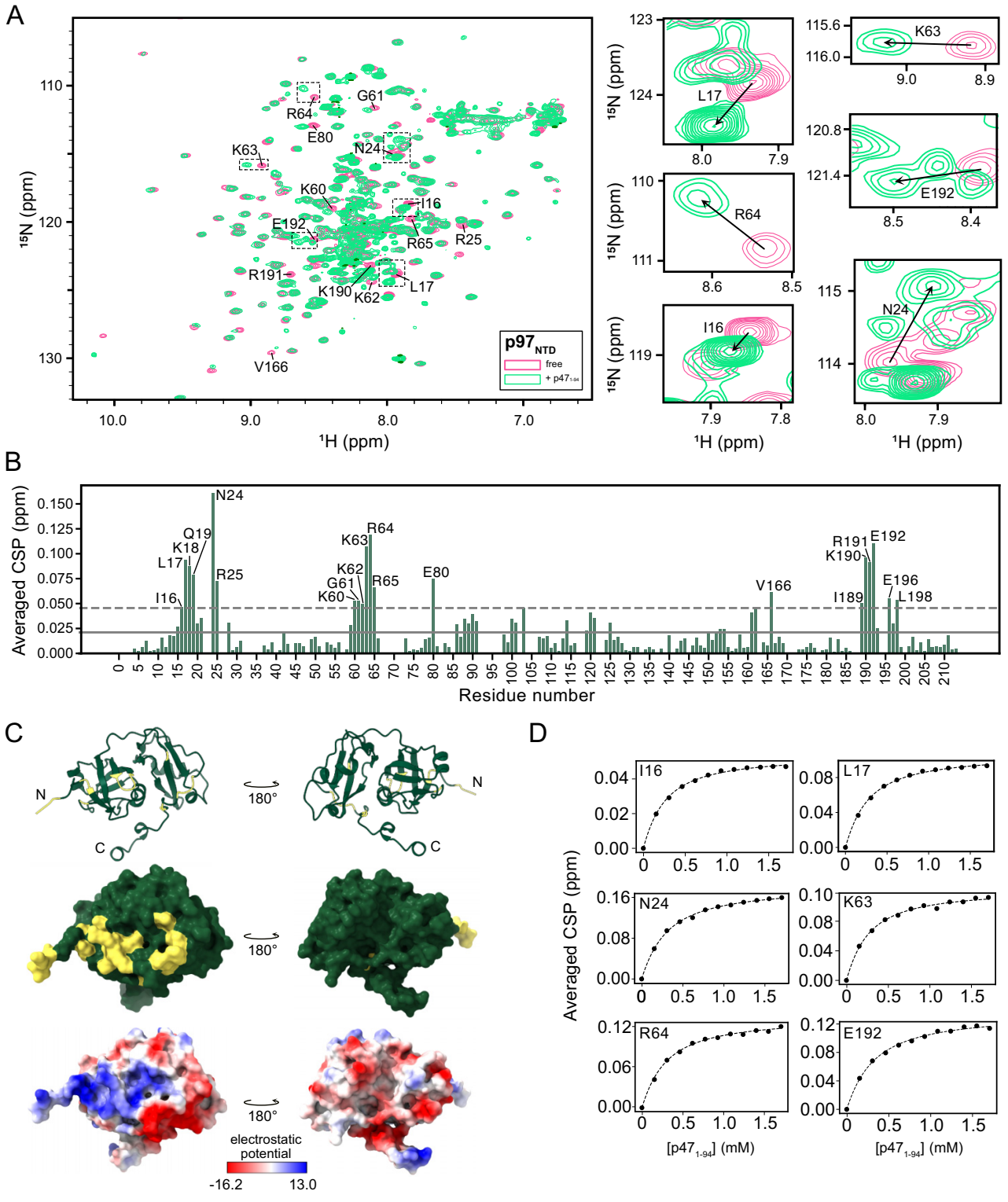

Fig. 4. Mapping the interaction site on $p97_{NTD}$ upon binding to $p47_{1–61}$. (A) Schematics of the construct of $p47_{1–61}$. (B) Chemical shift perturbations (CSPs) from ^{15}N-^{1}H HSQC spectra of $p97_{NTD}$ upon addition of $p47_{1–61}$. The average CSP value and CSP 1 STD above the average are indicated with solid and dashed lines, respectively. Residues with CSPs 1 STD above average are annotated. (C) Cartoon (top) and surface (bottom) representations of $p97_{NTD}$ (PDB ID code 1R7R[48], residue 1–213) with residues that show CSPs 1 STD above average in (B) colored in orange. The binding interface largely overlaps with the surface that binds $p47_{1–94}$. UBA, ubiquitin-associated; NTD, N-terminal domain.

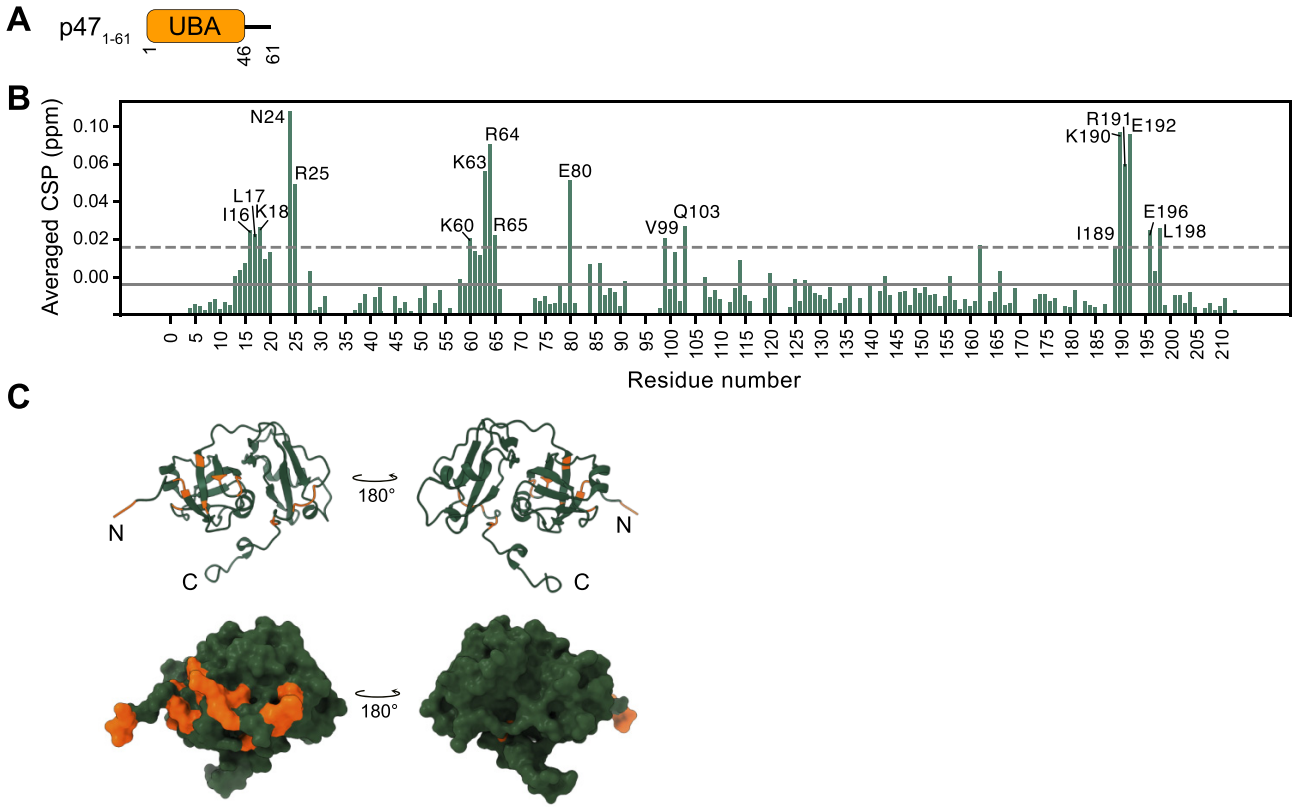

and D49) and a few acidic residues on the loop following α3 (i.e., D47 and D49) (Fig. 5B), which makes contacts with the basic residues on the N-lobe of $p97_{NTD}$ (including K18, N21, R22, R25, K62, K63, R64, and K60) (Fig. 5C). To generate a model for the $p47_{Site\ II}$ – $p97_{NTD}$ complex, we allowed residues 75–90 of $p47_{1–94}$ to be fully flexible during the docking protocol. The four best structures from the selected cluster are shown (Fig. 5D, top) with the lowest-energy structure in surface representation (Fig. 5D, bottom). The binding interface in the lowest-energy structure spans residues 75–85 in p47 (i.e., F75, L78, I79, H80, Q82, D83, E85, and E86) (Fig. 5E) and an extended basic region that spans both N- and C-lobes of $p97_{NTD}$ (i.e., R25, K62, K63, R93, R95, V99, R191, D193, E194, and E196) (Fig. 5F). The interfaces feature oppositely charged residues on p47 and p97, confirming the dominant role of electrostatic interaction for both binding events. Notably, a comparison of the binding interfaces on $p97_{NTD}$ reveals a more extended interaction area for the $p47_{Site\ II}$ – $p97_{NTD}$ complex (Fig. 5F), compared with that for the $p47_{Site\ I}$ – $p97_{NTD}$ complex (Fig. 5C). This is also consistent with a larger buried surface area for the $p47_{SiteII}$ – $p97_{NTD}$ complex (1663.0 Å) than for the $p47_{Site\ I}$ – $p97_{NTD}$ complex (1232.0 Å), which may explain the moderately higher apparent binding affinity for residues in Site II than those in Site I.

It is worth noting that the full-length p97 is arranged as a homo-hexamer, in which six NTDs reside on top of the D1 ring. The NTDs adopt two distinct conformations—the "up" and "down" conformations, dependent on the bound nucleotide (Figs. 6B and 6C).[12] We mapped the residues on $p97_{NTD}$ that show significant CSPs upon binding to $p47_{1–94}$ in the NMR titration experiment on both the "up" and "down" conformations of the hexameric p97 (Figs. 6B and 6C, cyan). Interestingly, the binding site is largely buried between the NTD-D1 domain interface in the ATP-bound state ("up" conformation), making it inaccessible to binding due to steric hindrance (Fig. 6B). On the other hand, in the ADP-bound state ("down" conformation), the binding interface is highly solvent exposed and is expected to be able to interact with both binding sites in $p47_{1–94}$ (Fig. 6C). This suggests that the interaction between $p97_{NTD}$ and $p47_{1–94}$ may be regulated by the nucleotide state of p97 and could vary at different stages of the catalytic cycle. Notably, the distance between the binding sites on the neighboring NTDs in the ADP-bound state is approximately 60 Å (Fig. 6C). Given the 30-residue long linker between the UBA domain and Site II, it is possible that Site I and Site II could interact with the neighboring NTDs on the same p97 hexamer simultaneously, and these interactions could potentially be cooperative between each other or

Fig. 5. Comparison of the structural models of $p47_{Site\ I}$ – $p97_{NTD}$ and $p47_{Site\ II}$ – $p97_{NTD}$ with the $p47_{UBA}$ – ubiquitin and $p97_{NTD}$ – $p47_{UBX}$ structures. (A) Ribbon (Top) and surface (Bottom) representation of the lowest-energy structural model of the complex between $p47_{Site\ I}$ and $p97_{NTD}$, with the interface residues on p47 and $p97_{NTD}$ annotated in (B) and (C), respectively. Only residues 1–49 of p47 were shown in (A) and (B). (D, top) Ribbon representations of the four best structural models of the complex between $p47_{Site\ II}$ and $p97_{NTD}$. The lowest-energy structure is shown in surface representation (D, bottom) with the interface residues on p47 and $p97_{NTD}$ annotated in (E) and (F), respectively. Only residues 71–94 of p47 were shown in (D) and (E). (G) Structural model of $p47_{UBA}$ – ubiquitin, generated by aligning $p47_{UBA}$ with the UBA domain of Dsk2p in the crystal structure of Dsk2p UBA – ubiquitin complex (PDB ID 1WR1)[47] (left). Residues of $p47_{UBA}$ that show significant nuclear magnetic resonance chemical shift perturbation upon interacting with ubiquitin are shown on the right[25], which partially overlapped with the surface of the UBA domain that interacts with $p97_{NTD}$. (H) Structures of the $p97_{NTD}$ – $p47_{UBX}$ (PDB ID 1S3S) (left, top) and $p97_{NTD}$ – SHP (PDB ID 5C1B) (left, bottom) complexes with the residues of $p97_{NTD}$ in the interaction interfaces annotated on the right. The $p97_{NTD}$ interfaces in these two complexes are distant from the surface that interacts with $p47_{1–94}$. Note that the $p97_{NTD}$s in (A), (C), (D), (F), and (H) are shown in the same view, while the $p47_{UBA}$ in (A), (B), and (G) are shown in the same view as well. NTD, N-terminal domain; UBA, ubiquitin-associated.

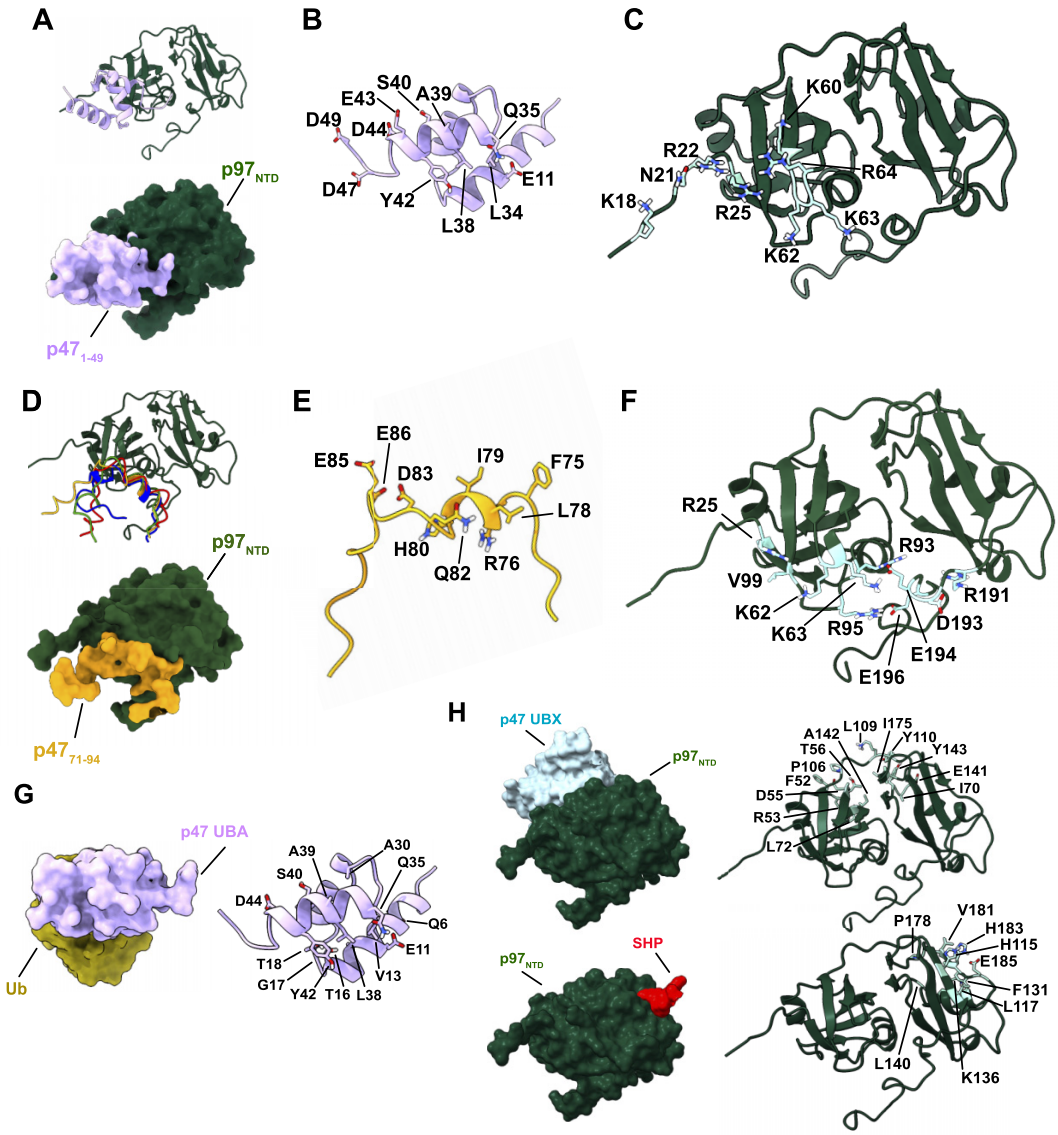

with previously characterized interactions between p97 and other motifs on the full-length p47, such as the UBX domain and the SHP_N and SHP_C motifs.

Interestingly, the interface on $p47_{UBA}$ in the $p47_{Site\ I}$ – $p97_{NTD}$ complex (Figs. 5A and 5B) partially overlaps with that in the $p47_{UBA}$ – ubiquitin complex[25,47] (Fig. 5G), suggesting that the binding of ubiquitin and $p97_{NTD}$ are mutually exclusive for a UBA domain. It has been reported that the interaction between $p47_{UBA}$ and ubiquitin plays an essential role in recruiting ubiquitinated substrates and delivering them to the p47–p97 complex for processing.[29,30] Since the binding affinity between $p47_{UBA}$ and ubiquitin is much stronger

Fig. 6. Binding interface on $p97_{NTD}$ mapped onto the hexameric p97 structure. (A) Domain arrangement of a p97 monomer. Surface representation of the full-length p97 hexamer in the "up" conformation (Apo/ATP-bound) (B) and the "down" conformation (ADP-bound) (C), with the residues that show significant chemical shift perturbations upon interacting with $p47_{1–94}$ (from Fig. 3B) colored in cyan. NTD, N-terminal domain.

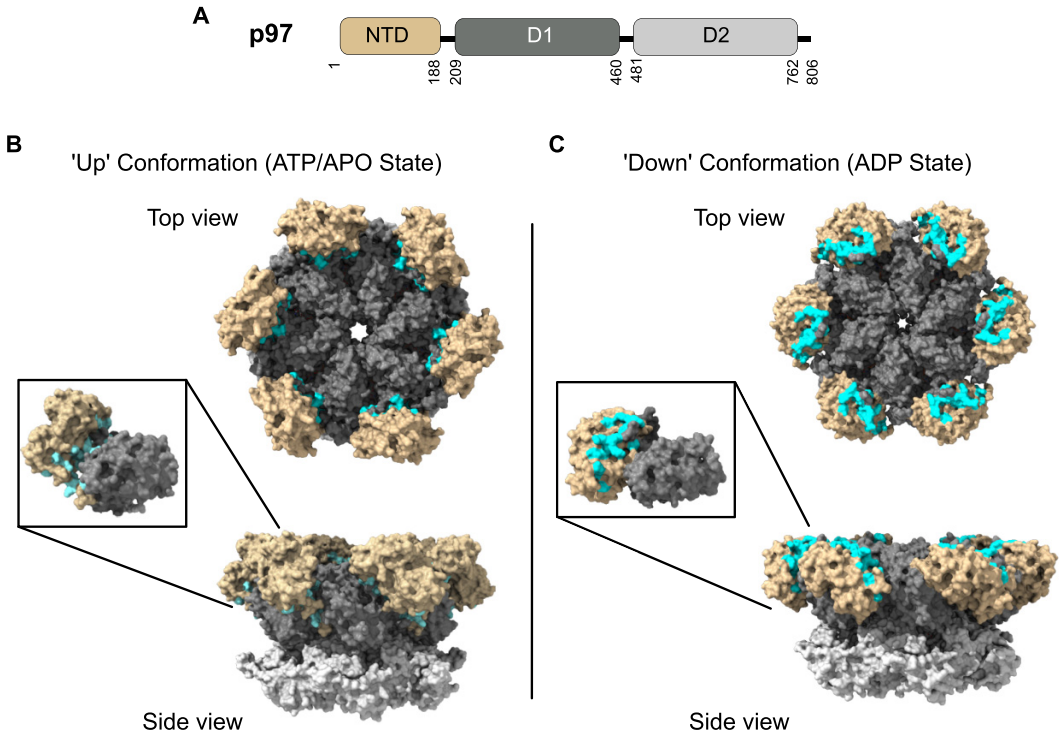

(K_d ~30 μM, data not shown) than that between $p47_{Site\ I}$ and $p97_{NTD}$, the interaction between $p47_{Site\ I}$ and $p97_{NTD}$ is likely to only occur when p47 is not loaded with ubiquitinated substrate (i.e., in the resting state), and the interaction breaks up upon binding of ubiquitin to $p47_{UBA}$. On the other hand, examining the interfaces on $p97_{NTD}$ reveals that the binding sites of Site I and Site II of p47 on $p97_{NTD}$ (Figs. 5C and 5F) are distant from the regions of NTD that interact with the UBX domain and the SHP motif (Fig. 5H), suggesting that Site I or Site II could potentially interact with an NTD that is already bound with a UBX domain and/or a SHP motif.

Previous studies have established that the UBA domain of p47 is responsible for recruiting ubiquitinated syntaxin5 to the p47–p97 complex to assist Golgi membrane reassembly.[29,30] Although it has been shown that p47 is anchored to the p97 hexamer via multiple interactions between the UBX domain/SHP motifs of p47 and p97 NTD, it is unclear how the UBA domain delivers the substrate to p97 given the long flexible linker between the UBA domain and the remainder of p47 (Fig. 1B, Linker 1). Direct interactions between the N-terminal part of p47 (including Site I and Site II) and p97, uncovered in this study, might play an important role in limiting the conformational freedom of the UBA domain with respect to p97 so as to assist in the delivery of substrates from UBA to the central pore of p97 for unfolding. It is plausible that the interaction between Site II and p97 NTD brings the UBA domain in close vicinity to the central pore of p97 for substrate processing. Meanwhile, binding of Site I to p97 NTD is probably regulated by substrate loading such that in the absence of ubiquitinated substrate, the interaction between Site I and p97 NTD confines the UBA domain close to the NTDs, while upon substrate binding the UBA domain disengages from p97 NTD to facilitate substrate translation. In general, our discovery of the new interactions between p47 and p97 emphasizes the multivalent binding mode in the p47–p97 complex and how linear motifs in intrinsically disordered linkers might play an important role in mediating and regulating the interactions in large biomolecular assemblies.

4. Conclusion

In this study we have discovered novel interactions between p47 and p97 that might have functional implications. Our NMR analysis revealed two acidic regions on the N-terminal fragment of p47, one located on α3 of the UBA domain (Site I) and the other spanning residues 69–94 on the linker (Site II), interact with the same basic surface on the NTD of p97. One of the interaction sites on p47 (Site II) has previously been shown to inhibit the ATPase activity of p97, which may result from a direct interaction with p97 NTD. Guided by NMR CSPs as restraints, we used the HADDOCK program to generate structural models for the complexes formed by Site I or Site II of p47 and the NTD of p97. The structural models confirmed that both interactions are driven by electrostatic force and revealed details of the potential binding interfaces. Comparison of the binding interfaces with

other previously characterized complexes shows compatibility of the different interactions that the interacting motifs might be involved in. For instance, the Site I – $p97_{NTD}$ interaction is not compatible with the substrate-loaded conformation of p47, while both Site I and Site II can bind to an NTD of p97 that is already bound with a UBX domain and/or a SHP motif of p47. The new interactions uncovered in this study highlight the multivalency in the p97–p47 complex[32] as well as in many other p97-adaptor complexes[4]. Intriguingly, these interactions may provide critical insights into how ubiquitinated substrates are delivered from p47 to p97 for translocation and unfolding.

Article information

History dates

Received: 8 September 2023
Accepted: 14 November 2023
Accepted manuscript online: 21 November 2023
Version of record online: 10 January 2024

Notes

This paper is part of a Special Issue entitled "Highlighting Excellence in Canadian Undergraduate Chemistry Research".

Copyright

Data availability

All data discussed in the paper will be made available to readers upon request.

Author information

Author ORCIDs

Peter Kim https://orcid.org/0000-0002-1724-8956
Megan Black https://orcid.org/0000-0001-5006-5337
Rui Huang https://orcid.org/0000-0002-4064-6397

Author notes

Peter Kim and Megan Black contributed equally to this work.

Author contributions

Conceptualization: RH
Data curation: PK, MB
Formal analysis: PK, RH
Funding acquisition: RH
Investigation: PK, RH
Methodology: FP, RH
Project administration: RH
Resources: RH
Software: FP
Supervision: RH
Validation: RH
Visualization: PK, MB
Writing – original draft: PK, MB, RH
Writing – review & editing: PK, MB, RH

Competing interests

The authors declare no conflict of interest.

Funding information

This research was funded by the the Natural Sciences and Engineering Research Council of Canada (NSERC) Discovery Grant. Student PK was supported by an Undergraduate Research Assistantship at the University of Guelph. MB was partially supported by Undergraduate Student Research Awards (USRA) program by NSERC.

Supplementary material

Supplementary data are available with the article at https://doi.org/10.1139/cjc-2023-0160.

References

(1) Christianson, J. C.; Ye, Y. Nat. Struct. Mol. Biol. **2014**, *21*(4), 325. doi:10.1038/nsmb.2793. PMID: 24699081.
(2) van den Boom, J.; Meyer, H. Mol. Cell, **2018**, *69*(2), 182. doi:10.1016/j.molcel.2017.10.028. PMID: 29153394.
(3) Stach, L.; Freemont, P. S. Biochem. J. **2017**, *474*(17), 2953. doi:10.1042/BCJ20160783. PMID: 28819009.
(4) Braxton, J. R.; Southworth, D. R. J. Biol. Chem. **2023**, 105182. doi:10.1016/j.jbc.2023.105182. PMID: 37611827.
(5) Costantini, S.; Capone, F.; Polo, A.; Bagnara, P.; Budillon, A. Int. J. Mol. Sci. **2021**, *22*(18), 10177. doi:10.3390/ijms221810177. PMID: 34576340.
(6) Bastola, P.; Oien, D. B.; Cooley, M.; Chien, J. AAPS J. **2018**, *20*(6). doi:10.1208/s12248-018-0254-1. PMID: 30151644.
(7) Huryn, D. M.; Kornfilt, D. J. P.; Wipf, P. J. Med. Chem. **2020**, *63*(5), 1892. doi:10.1021/acs.jmedchem.9b01318. PMID: 31550150.
(8) Watts, G. D. J.; Wymer, J.; Kovach, M. J.; Mehta, S. G.; Mumm, S.; Darvish, D.; Pestronk, A.; Whyte, M. P.; Kimonis, V. E. Nat. Genet. **2004**, *36*(4), 377. doi:10.1038/ng1332. PMID: 15034582.
(9) Johnson, J. O.; Mandrioli, J.; Benatar, M.; Abramzon, Y.; Van Deerlin, V. M.; Trojanowski, J. Q.; Gibbs, J. R.; Brunetti, M.; Gronka, S.; Wuu, J.; Ding, J.; McCluskey, L.; Martinez-Lage, M.; Falcone, D.; Hernandez, D. G.; Arepalli, S.; Chong, S.; Schymick, J. C.; Rothstein, J.; Landi, F.; Wang, Y. D.; Calvo, A.; Mora, G.; Sabatelli, M.; Monsurrò, M. R.; Battistini, S.; Salvi, F.; Spataro, R.; Sola, P.; Borghero, G.; Galassi, G.; Scholz, S. W.; Taylor, J. P.; Restagno, G.; Chiò, A.; Traynor, B. J. Neuron, **2010**, *68*(5), 857. doi:10.1016/j.neuron.2010.11.036. PMID: 21145000.
(10) Darwich, N. F.; Phan, J. M.; Kim, B.; Suh, E.; Papatriantafyllou, J. D.; Changolkar, L.; Nguyen, A. T.; O'Rourke, C. M.; He, Z.; Porta, S.; Gibbons, G. S.; Luk, K. C.; Papageorgiou, S. G.; Grossman, M.; Massimo, L.; Irwin, D. J.; McMillan, C. T.; Nasrallah, I. M.; Toro, C.; Aguirre, G. K.; Van Deerlin, V. M.; Lee, E. B. Science, **2020**, *370*(6519). doi:10.1126/science.aay8826.
(11) Gonzalez, M. A.; Feely, S. M.; Speziani, F.; Strickland, A. V.; Danzi, M.; Bacon, C.; Lee, Y.; Chou, T. F.; Blanton, S. H.; Weihl, C. C.; Zuchner, S.; Shy, M. E. Brain, **2014**, *137*(11), 2897. doi:10.1093/brain/awu224. PMID: 25125609.
(12) Banerjee, S.; Bartesaghi, A.; Merk, A.; Rao, P.; Bulfer, S. L.; Yan, Y.; Green, N.; Mroczkowski, B.; Neitz, R. J.; Wipf, P.; Falconieri, V.; Deshaies, R. J.; Milne, J. L. S.; Huryn, D.; Arkin, M.; Subramaniam, S. Science, **2016**, *351*(6275), 871. doi:10.1126/science.aad7974. PMID: 26822609.
(13) Schuller, J. M.; Beck, F.; Lössl, P.; Heck, A. J. R.; Förster, F. FEBS Lett. **2016**, *590*(5), 595. doi:10.1002/1873-3468.12091. PMID: 26849035.
(14) Xu, Y.; Han, H.; Cooney, I.; Guo, Y.; Moran, N. G.; Zuniga, N. R.; Price, J. C.; Hill, C. P.; Shen, P. S. Nat. Commun. **2022**, *13*(1), 1. doi:10.1038/s41467-022-30318-3. PMID: 34983933.
(15) Cooney, I.; Han, H.; Stewart, M. G.; Carson, R. H.; Hansen, D. T.; Iwasa, J. H.; Price, J. C.; Hill, C. P.; Shen, P. S. Science, **2019**, *365*(6452), 502. doi:10.1126/science.aax0486.

(16) Twomey, E.; Ji, Z.; Wales, T. E.; Bodnar, N. O.; Ficarro, S. B.; Marto, J. A.; Engen, J. R.; Rapoport, T. A. Science, **2019**, *365*(6452), eaax1033. doi:10.1126/science.aax1033. PMID: 31249135.
(17) Pan, M.; Yu, Y.; Ai, H.; Zheng, Q.; Xie, Y.; Liu, L.; Zhao, M. bioRxiv, **2021**, 2021.02.08.430295. doi:10.1101/2021.02.08.430295.
(18) Puchades, C.; Sandate, C. R.; Lander, G. C. Nat. Rev. Mol. Cell Biol. **2020**, *21*(1), 43. doi:10.1038/s41580-019-0183-6. PMID: 31754261.
(19) Ye, Y.; Tang, W. K.; Zhang, T.; Xia, D. Front. Mol. Biosci. **2017**, *4*, 39. doi:10.3389/fmolb.2017.00039. PMID: 28660197.
(20) Hänzelmann, P.; Schindelin, H. **2017**, *4*(April), 1. doi:10.3389/fmolb.2017.00021.
(21) Buchberger, A.; Schindelin, H.; Hänzelmann, P. FEBS Lett. **2015**, *589*(19), 2578. doi:10.1016/j.febslet.2015.08.028. PMID: 26320413.
(22) Rabouille, C.; Levine, T. P.; Peters, J. M.; Warren, G. Cell, **1995**, *82*(6), 905. doi:10.1016/0092-8674(95)90270-8. PMID: 7553851.
(23) Kondo, H.; Rabouille, C.; Newman, R.; Levine, T. P.; Pappin, D.; Freemont, P.; Warren, G. Nature, **1997**, *388*(6637), 75. doi:10.1038/40411. PMID: 9214505.
(24) Uchiyama, K.; Kondo, H. J. Biochem. **2005**, *137*(2), 115–119. doi:10.1093/jb/mvi028. PMID: 15749824.
(25) Yuan, X.; Simpson, P.; McKeown, C.; Kondo, H.; Uchiyama, K.; Wallis, R.; Dreveny, I.; Keetch, C.; Zhang, X.; Robinson, C.; Freemont, P.; Matthews, S. EMBO J. **2004**, *23*(7), 1463. doi:10.1038/sj.emboj.7600152. PMID: 15029246.
(26) Soukenik, M.; Diehl, A.; Leidert, M.; Sievert, V.; Büssow, K.; Leitner, D.; Labudde, D.; Ball, L. J.; Lechner, A.; Nägler, D. K.; Oschkinat, H. FEBS Lett. **2004**, *576*(3), 358. doi:10.1016/j.febslet.2004.09.037. PMID: 15498563.
(27) Yuan, X.; Shaw, A.; Zhang, X.; Kondo, H.; Lally, J.; Freemont, P. S.; Matthews, S. J. Mol. Biol. **2001**, *311*(2), 255. doi:10.1006/jmbi.2001.4864. PMID: 11478859.
(28) Dreveny, I.; Kondo, H.; Uchiyama, K.; Shaw, A.; Zhang, X.; Freemont, P. S. EMBO J. **2004**, *23*(5), 1030. doi:10.1038/sj.emboj.7600139. PMID: 14988733.
(29) Meyer, H. H.; Wang, Y.; Warren, G. EMBO J. **2002**, *21*(21), 5645. doi:10.1093/emboj/cdf579. PMID: 12411482.
(30) Huang, S.; Tang, D.; Wang, Y. Dev. Cell, **2016**, *38*(1), 73. doi:10.1016/j.devcel.2016.06.001. PMID: 27404360.
(31) Weith, M.; Seiler, J.; van den Boom, J.; Kracht, M.; Hülsmann, J.; Primorac, I.; del Pino Garcia, J.; Kaschani, F.; Kaiser, M.; Musacchio, A.; Bollen, M.; Meyer, H. Mol. Cell, **2018**, *72*(4), 766. doi:10.1016/j.molcel.2018.09.020. PMID: 30344098.
(32) Conicella, A. E.; Huang, R.; Ripstein, Z. A.; Nguyen, A.; Wang, E.; Löhr, T.; Schuck, P.; Vendruscolo, M.; Rubinstein, J. L.; Kay, L. E. Proc. Natl. Acad. Sci. U.S.A. **2020**, *117*(42), 26226. doi:10.1073/pnas.2013920117. PMID: 33028677.
(33) Zhang, X.; Gui, L.; Zhang, X.; Bulfer, S. L.; Sanghez, V.; Wong, D. E.; Lee, Y.; Lehmann, L.; Lee, J. S.; Shih, P.-Y.; Lin, H. J.; Iacovino, M.; Weihl, C. C.; Arkin, M. R.; Wang, Y.; Chou, T.-F. Proc. Natl. Acad. Sci. U.S.A. **2015**, *112*(14), E1705. doi:10.1073/pnas.1418820112. PMID: 25775548.
(34) Schuetz, A. K.; Kay, L. E. Elife, **2016**, *5*, e20143. doi:10.7554/eLife.20143. PMID: 27828775.
(35) Delaglio, F.; Grzesiek, S.; Vuister, G. W.; Zhu, G.; Pfeifer, J.; Bax, A. J. Biomol. NMR, **1995**, *6*(3), 277. doi:10.1007/BF00197809. PMID: 8520220.
(36) Lee, W.; Tonelli, M.; Markley, J. L. Bioinformatics, **2015**, *31*(8), 1325. doi:10.1093/bioinformatics/btu830. PMID: 25505092.
(37) Williamson, M. P. Mod. Magn. Reson. **2018**, 995. doi:10.1007/978-3-319-28388-376.
(38) Paszke, A.; Gross, S.; Massa, F.; Lerer, A.; Bradbury, J.; Chanan, G.; Killeen, T.; Lin, Z.; Gimelshein, N.; Antiga, L.; Desmaison, A.; Köpf, A.; Yang, E.; DeVito, Z.; Raison, M.; Tejani, A.; Chilamkurthy, S.; Steiner, B.; Fang, L.; Bai, J.; Chintala, S. PyTorch: An Imperative Style, High-Performance Deep Learning Library. **2019**.
(39) Press, W. H.; Flannery, B. P.; Teukolsky, S. A.; Vetterling, W. T. Numerical Recipes in C. Cambridge University Press, **1998**.
(40) Honorato, R. V.; Koukos, P. I.; Jiménez-García, B.; Tsaregorodtsev, A.; Verlato, M.; Giachetti, A.; Rosato, A.; Bonvin, A. M. J. J. Front. Mol. Biosci. **2021**, *8*(July), 1. doi:10.3389/fmolb.2021.729513.
(41) Van Zundert, G. C. P.; Rodrigues, J. P. G. L. M.; Trellet, M.; Schmitz, C.; Kastritis, P. L.; Karaca, E.; Melquiond, A. S. J.; Van Dijk, M.; De Vries, S. J.; Bonvin, A. M. J. J. J. Mol. Biol. **2016**, *428*(4), 720. doi:10.1016/j.jmb.2015.09.014. PMID: 26410586.
(42) Huyton, T.; Pye, V. E.; Briggs, L. C.; Flynn, T. C.; Beuron, F.; Kondo, H.; Ma, J.; Zhang, X.; Freemont, P. S. J. Struct. Biol. **2003**, *144*(3), 337. doi:10.1016/j.jsb.2003.10.007. PMID: 14643202.
(43) Tunyasuvunakool, K.; Adler, J.; Wu, Z.; Green, T.; Zielinski, M.; Žídek, A.; Bridgland, A.; Cowie, A.; Meyer, C.; Laydon, A.; Velankar, S.; Kleywegt, G. J.; Bateman, A.; Evans, R.; Pritzel, A.; Figurnov, M.; Ronneberger, O.; Bates, R.; Kohl, S. A. A.; Potapenko, A.; Ballard, A. J.; Romera-Paredes, B.; Nikolov, S.; Jain, R.; Clancy, E.; Reiman, D.; Petersen, S.; Senior, A. W.; Kavukcuoglu, K.; Birney, E.; Kohli, P.; Jumper, J.; Hassabis, D. Nature, **2021**. doi:10.1038/s41586-021-03828-1.
(44) Bodnar, N. O.; Rapoport, T. A. Cell, **2017**, *169*(4), 722. doi:10.1016/j.cell.2017.04.020. PMID: 28475898.
(45) Rao, M. V; Williams, D. R.; Cocklin, S.; Loll, P. J. J. Biol. Chem. **2017**, *292*(45), 18392. doi:10.1074/jbc.M117.806281. PMID: 28939772.
(46) Bulfer, S. L.; Chou, T. F.; Arkin, M. R. ACS Chem. Biol. **2016**, *11*(8), 2112. doi:10.1021/acschembio.6b00350. PMID: 27267671.
(47) Ohno, A.; Jee, J.; Fujiwara, K.; Tenno, T.; Goda, N.; Tochio, H.; Kobayashi, H.; Hiroaki, H.; Shirakawa, M. Structure, **2005**, *13*(4), 521. doi:10.1016/j.str.2005.01.011. PMID: 15837191.
(48) Goddard, T. D.; Huang, C. C.; Ferrin, T. E. J. Struct. Biol. **2007**, *157*(1), 281. doi:10.1016/j.jsb.2006.06.010. PMID: 16963278.
(49) Huyton, T.; Pye, V. E.; Briggs, L. C.; Flynn, T. C.; Beuron, F.; Kondo, H.; Ma, J.; Zhang, X.; Freemont, P. S. J. Struct. Biol. **2003**, *144*(3), 337. doi:10.1016/j.jsb.2003.10.007. PMID: 14643202.